Journal of Physics and Chemistry of Solids 160 (2022) 110345

Contents lists available at ScienceDirect

Journal of Physics and Chemistry of Solids

journal homepage: www.elsevier.com/locate/jpcs

A first principles study on electrochemical sensing of highly toxic pesticides by using porous C_4N nanoflake

Misbah Asif [a], Hasnain Sajid [b], Khurshid Ayub [a], Muhammad Ans [c], Tariq Mahmood [a,*]

[a] Department of Chemistry, COMSATS University Islamabad, Abbottabad Campus, Abbottabad, 22060, Pakistan
[b] School of Science and Technology, Nottingham Trent University, Clifton Lane, Nottingham, NG11 8NS, UK
[c] Department of Chemistry, University of Agriculture, Faisalabad, Punjab, Pakistan

ARTICLE INFO

Keywords:
C_4N nanoflake
Pesticides
Sensing
Density functional theory

ABSTRACT

C_4N is a novel porous two-dimensional material with fascinating electronic and chemical properties. Thereby, the sensing ability of C_4N is the most aspect topic of research nowadays. In this study, potential application of C_4N nanoflake as a chemical sensor for the toxic pesticides has been investigated using density functional theory calculations. The sensing ability of C_4N for pesticides is evaluated through the interaction energy, noncovalent interaction index (NCI), quantum theory of atoms in molecule (QTAIM), molecular orbitals and CHELPG charge transfer analyses. The first principle calculations on ωB97XD/6-31G(d, p) level of DFT show that the C_4N is selectively sensitive to Dichlorodiphenyltrichloroethane (DDT), Fenitrothion (FNT), Dimethoxy (DMDT), Ronnel (RN) and Fenthion (FT). The interaction of pesticides leads to the significant changes in the electronic structure of C_4N. The observed sequence of interaction energy of our reported complexes is DDT@C_4N > FNT@C_4N > DMDT@C_4N > RN@C_4N > FT@C_4N. The electronic structure changes can be demonstrated from two aspects: the strong interaction between pesticide molecule and C_4N, the variation in HOMO-LUMO orbital energies and charge transfer from C_4N to pesticide. The charges distribution between analytes and C_4N nanoflake on interaction is analyzed by the electron density differences (EDD) and charge decomposition analysis (CDA). Our results reveal the potential application of C_4N in electronic and sensor devices especially for the detection of toxic chemicals.

1. Introduction

Chemical sensors are important devices that are used extensively for the detection of environmental pollutants [1–4]. From the last few decades, covalent organic frameworks [5,6], metal-organic frameworks [7–9], metal oxides [10,11], graphene [4,12], clusters [13,14] and 2-dimensional (2D) sheets [15,16] are extensively explored materials in sensor devices. Owing to their high sensitivity, selectivity and quick response, these materials have attracted the attention of the scientific community. This might be due to the high chemical & mechanical stability and extraordinary optical and electrical properties of carbon nitride sheets. Literature reveals that the C_2N and C_3N have been widely studied in gas sensing applications [17–19]. For example, Yar et al. [20], used C_2N for selective detection of NH_3 and H_2S from a mixture of warfare agents (NH_3, PH_3, NF_3, NCl_3, H_2S, HCN and $COCl_3$). Another report explored the sensitivity and selectivity of C_3N sensor toward NO_3, SO_3, NO and NO_2 gases [18]. These and many other studies [19,21–23] attribute the high sensing abilities of C_2N and C_3N sheets toward gaseous molecules. However, the sensing utility of their novel analogue i.e., C_4N still needs to be explored. Although, C_4N is not explored as a gas sensor, however, it has been applied in various other fields. Recently, Li et al. used C_4N as a catalyst for oxygen reduction reaction [24].

In 2020, C_4N is firstly reported by Li et al. [24], and postulated that C_4N is a conjugated nonmetallic organic polymer with a thin sheet-like structure containing repeating pyrazine units. The mechanical and electronic structures of C_4N is confirmed by various experimental techniques such as fourier transform infrared (FT-IR) and nuclear magnetic resonance (NMR) [24]. C_4N exhibits high chemical stability, great thermal resistance, extraordinary charge transport properties due to the π-conjugated system. Pyrazine nitrogen in C_4N triggers the intramolecular charge transfer which enhances the binding affinities of C_4N for various foreign entities [24]. In this study, we became interested in exploring the sensing ability of C_4N for toxic pesticides.

Extensive use of agrochemicals (pesticides) to prevent agriculture

* Corresponding author.
E-mail address: mahmood@cuiatd.edu.pk (T. Mahmood).

https://doi.org/10.1016/j.jpcs.2021.110345
Received 4 March 2021; Received in revised form 24 June 2021; Accepted 15 August 2021
Available online 18 August 2021

energetic, electronic, and optical properties.

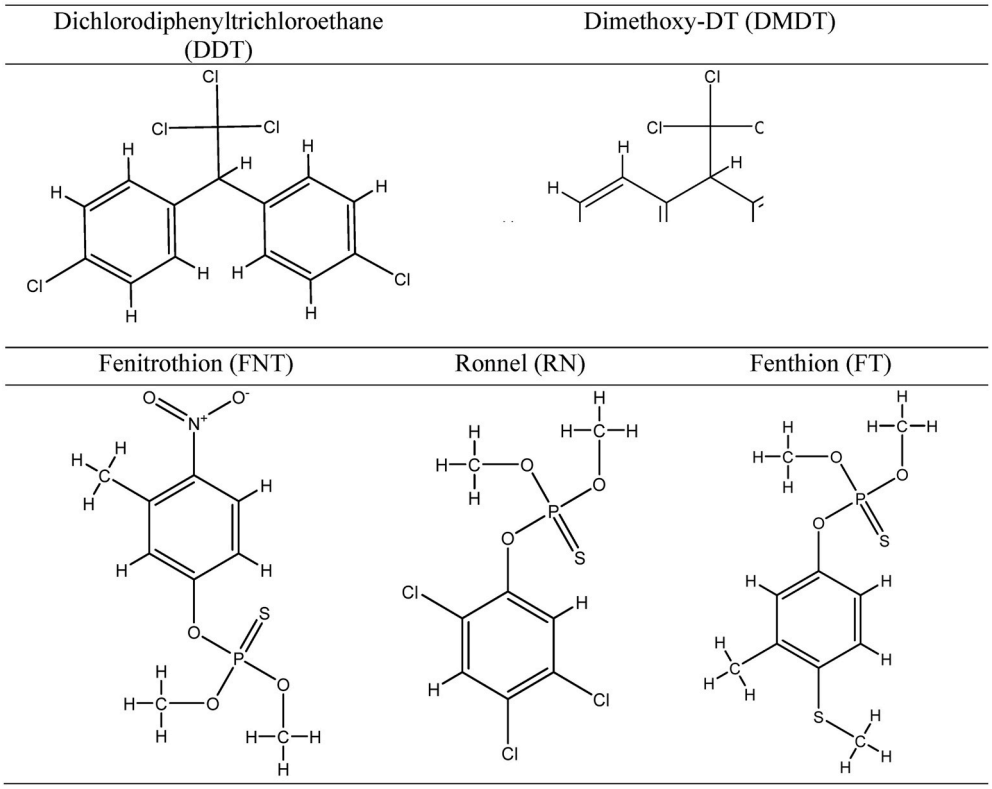

Fig. 1. Molecular structures of Dichlorodiphenyltrichloroethane (DDT), Dimethoxy-DDT (DMDT), Fenitrothion (FNT), Ronnel (RN) and Fenthion (FT).

crops from insects and pests to increase the yield has led to environmental pollution with toxic residues. According to the research of Pimentel et al., only 0.3% of applied pesticides are used for pest killing while about 99.7% are mixed with the environmental gases [25]. Thus, pesticides poisoning accounts for approximately 300,000 deaths annually [26]. The pesticides cause many disorders including cancer, neurological, respiratory, reproductive, endocrine and DNA damage [27–30]. Generally, pesticides are divided into different classes based on the mode of action i.e., herbicides, fungicides, insecticides, *etc*. While, based on their chemical structures, pesticides are classified as, organophosphates, carbamates, organochlorines *etc*. Among them, the organophosphate and organochloride pesticides namely, Dichlorodiphenyltrichloroethane (DDT), Fenitrothion (FNT), Dimethoxy (DMDT), Ronnel (RN) and Fenthion (FT) (Fig. 1), cause a more drastic effect on the living organisms [36]. For instance, Fenitrothion, Dimethoxy, Ronnel and Fenthion show some genotoxic effects and also cause cardiovascular diseases, dementia, and neurological disorders [31]. Moreover, DDT exposure can cause tremors, paralysis, excitability, muscle twitch, anemia, vomiting, seizures, nausea, hyperpyrexia, ataxia, and many others in humans [32]. Many studies reveal that the most chronic effect of these pesticides especially DDT on the female is breast cancer [33–35]. FNT produces cytotoxic effects on the liver and lungs of patients which ultimately causes death [36]. The chronic effects of DMDT, RN and FT are similar to those caused by DDT and FNT. Therefore, the detection of these toxic molecules in the topic of significant scientific interest.

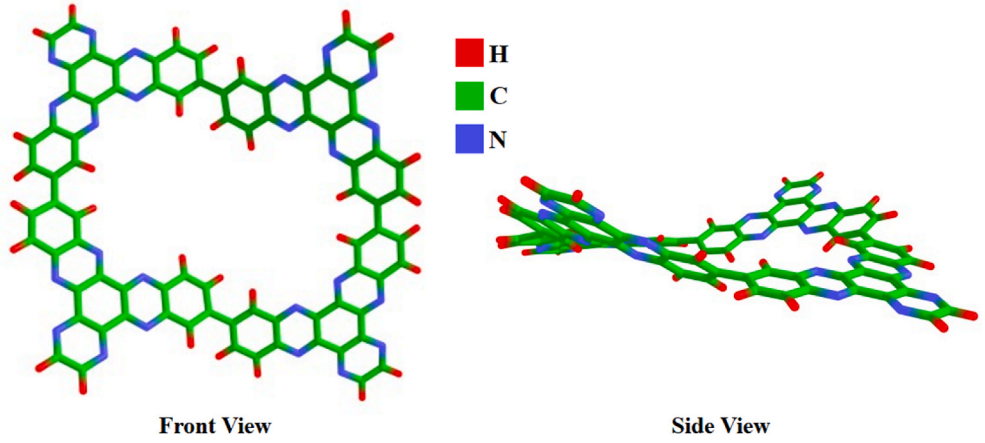

Fig. 2. Optimized structure of C_4N (Front view and Side view).

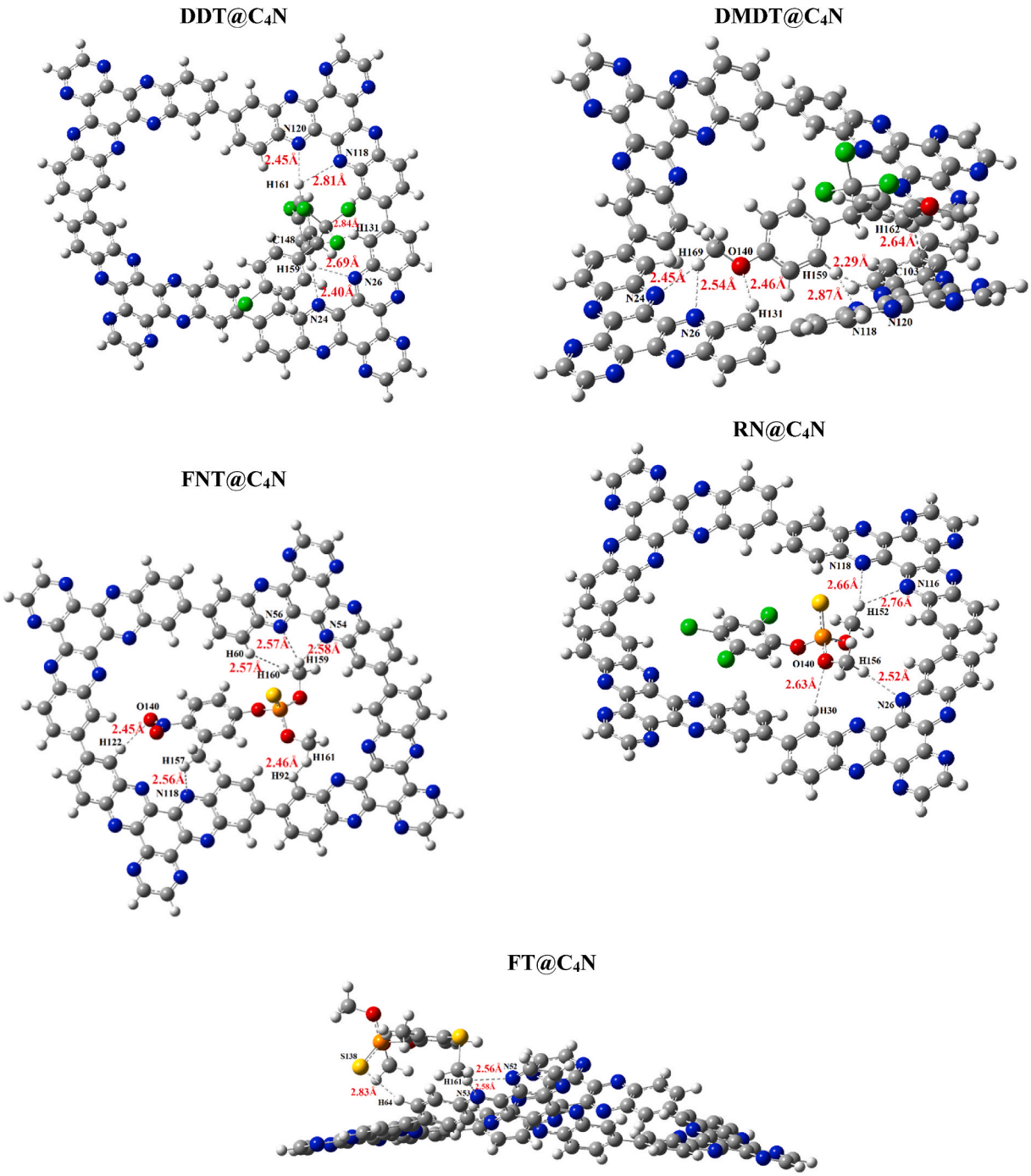

Fig. 3. The optimized geometries of DDT@C_4N, FNT@C_4N, DMDT@C_4N, RN@C_4N and FT@C_4N complexes with interacting distance (D_{int}) (Where grey: C, white: H, red: O, yellow: S, orange: P, green: Cl, and blue: N).

Although, the 2D carbon sheets [37], metal oxide [38,39], synthetic polymers [40] have been used for the sensing of toxic chemicals as well as organophosphate pesticides. However, the research to explore the best sensor material with excellent sensitivity for the detection of toxic chemicals is still under investigation. Recently, graphene-like heteroatomic nanomaterials such as phosphorene [41,42], tellurene [43], bismuthine [44], arsenene [45] have attracted great attentions of researcher due to their high mechanical strength and fascinating electronic properties. On the other side, significant efforts have been made to improve the semiconducting properties of graphene by controlling construction of 2D nitrogenated holey graphene [46] i.e., C_2N and C_3N, *etc*. The C_4N is quite comparable to that of holey graphene analogues because the hybridization of C/N atoms of C_4N is sp^3 and the remarkable band structure with the Fermi velocity of 2.6×10^5 m/s at the Dirac cone [47]. Thus, the researchers claimed that C_4N is a promising material for applications in high speed opto-electric devices. Here, we explore the sensitivity and selectivity of C_4N towards toxic pesticides via geometric, energetic, electronic, and optical properties.

2. Computational methodology

All calculations are performed at Gaussian09 [48] software while the results are analyzed by GassView5.0 [49] software. For comparison, ωB97XD and M052X-D3 (employing Becke Johnson damping (BJ))

Table 1
Counterpoise corrected interaction energies (E_{cp}) in unit of kcal/mol, interacting atoms (A_{int}), interacting distance (D_{int}) of analytes@C_4N complexes.

Analyte@C_4N	A_{int}	D_{int} (Å)	E_{cp} (WB97XD)	E_{cp} (M052X)
DDT@C_4N	H_{159}–N_{24}	2.40	−24.37	−21.77
	H_{161}–N_{120}	2.45		
	H_{159}–N_{26}	2.69		
	H_{161}–N_{118}	2.81		
	C_{148}–H_{131}	2.84		
FNT@C_4N	O_{140}–H_{122}	2.45	−21.79	−21.70
	H_{157}–N_{118}	2.56		
	H_{159}–N_{56}	2.57		
	H_{159}–N_{54}	2.58		
DMDT@C4N	H_{150}–N_{120}	2.29	−21.43	−18.27
	H_{169}–N_{24}	2.45		
	O_{140}–H_{131}	2.46		
	H_{169}–N_{26}	2.54		
	H_{162}–C_{103}	2.64		
	H_{159}–N_{118}	2.87		
RN@C_4N	H_{156}–N_{26}	2.52	−19.90	−19.39
	O_{140}–H_{30}	2.63		
	H_{152}–N_{118}	2.66		
	H_{152}–N_{116}	2.76		
FT@C_4N	H_{161}–N_{52}	2.56	−15.29	−13.37
	H_{161}–N_{53}	2.58		
	S_{138}–H_{64}	2.83		

functionals along with 6–31G(d, p) basis set are used for geometry optimization of pure C_4N (Fig. 2) and all the respective complexes with selected pesticides (Fig. 3). ωB97XD is a hybrid DFT, long-range dispersion corrected functional which performs exceptionally well for noncovalent interacting systems [50–52]. On the other hand, M05–2X is also a well know functional for noncovalent interaction with double nonlocal exchange contribution [53], however, Grimme's dispersion (D3BJ) has also added to further refine the interaction energies [54]. The interaction energies of the optimized complexes are calculated by the expression below:

$$E_{int} = E_{analytes@C4N} - (E_{C4N} + E_{analytes}) + BSSE \quad (1)$$

Where, $E_{analytes@C4N}$, E_{C4N}, $E_{analytes}$ represent the energies of complex, surface (C_4N) and individual analytes (pesticide), respectively. The counterpoise method is implemented to remove basis set superposition error (BSSE), which arises due to overlapping of finite basis set. In order to investigate the nature and strength of interactions between C_4N and Pesticides, noncovalent interaction index (NCI) and quantum theory of atoms in molecules (QTAIM) analyses are performed using Multiwfn3.6 software [55]. The electronic response of C_4N toward pesticide molecule is measured by calculating the variation of electronic properties upon complexation. The electronic properties including HOMO-LUMO gap and NBO charge transfer are calculated at ωB97XD/6-31G(d, p) level of theory. The density of state analysis is also performed via GaussSum package [56], for the confirmation of shifting of orbitals on interaction with pesticide molecules. Furthermore, the charge decomposition analysis (CDA) is performed to quantify the donor-acceptor relationship between the interacting analytes and C_4N. Lastly, time-dependent density functional theory (TD-DFT) calculations are performed to study the variation in the optical properties of C_4N on interaction with pesticides.

3. Results and discussions

3.1. Optimized geometries and their stability

The analytes including DDT, DMDT, FNT, RN and FT are adsorbed on C_4N surface which result five complexes namely, DDT@C_4N, DMDT@C_4N, FNT@C_4N, RN@C_4N and FT@C_4N, respectively. A number of orientations of each analyte on C_4N are studied to get the most stable geometries. These orientations are carefully and judiciously built by evaluating electrophilic and nucleophilic sites of C_4N and analytes from molecular electrostatic potentials (MESP) analysis (see Fig. S1). Thus, the geometries are constructed in such a way that the electrophilic site of pesticides sits on the nucleophilic site of C_4N, vice versa. The most stable complexes are displayed in Fig. 3 while the other possible interaction geometries with their relative energies (Hartree) are given in supplementary information (Figs. S2–S6). As mentioned above, the BSSE corrected energies of all the complexes are calculated at ωB97XD and M052X-D3 functionals for a better analysis of interaction stabilities. The counterpoise interaction energies of complexes are listed in Table 1. Expectedly, the complexes reflect the higher stability at ωB97XD/6-31G (d, p) level of theory, however, the trend of interaction stability of complexes is quite comparable in the both functionals. The discussion is limited only to the results generated at ωB97XD functional.

Like interaction energies (E_{int}), the interaction distances (D_{int}) play a pivotal role in describing the interaction strength and behavior. These interaction parameters of the stable complexes are also listed in Table 1. Although, there are multiple interactions possible, but the discussion is only limited to the least interaction distance for the ease of understanding. The results reveal that the interaction energy of the DDT@C_4N complex is the highest which illustrates the high sensitivity of C_4N towards DDT. The E_{int} of the DDT@C_4N complex is −24.37 kcal/mol along with the interaction distance of 2.40 Å between the H_{159} and N_{24} (refer to Fig. 3). Among various interaction distances (listed in Table 1), the discussion is only made on the least distance between analytes and C_4N. The structure of the DDT@C_4N complex in Fig. 3 illustrates that the molecule of DDT shows maximum interaction with a single unit of C_4N which might be due to the high flexibility and the torsion between the aromatic rings of the DDT molecule [32]. The next highest interaction energy is calculated for FNT@C_4N complex that is −21.79 kcal/mol. The small interaction distance (2.45 Å) between O_{140} of FNT and H_{122} of C_4N results in higher stability of the complex. The higher stability of the FNT@C_4N complex might be due to the maximum interaction between FNT and C_4N. The molecular size of FNT is 9.94 Å and it can be easily accomodated in the cavity of C_4N with the pore size of 13.97 Å. Moreover, the terminal oxygen atoms of the nitro group at the para position of the aromatic ring of FNT enhances the interaction stability of FNT@C_4N complex.

The thermodynamic stability of FNT@C_4N is followed by the DMDT@C_4N complex. The interaction energy and the interaction distance (H_{150}–N_{120}) in the DMDT@C_4N complex are −21.43 kcal/mol and 2.29 Å, respectively. The DMDT molecule cannot fully accommodate in the cavity of C_4N due to the large size of the molecule which might be the reason for decreasing interaction stability as compared to the DDT@C_4N and FNT@C_4N. Lastly, the RN@C_4N and FT@C_4N complexes show the least stability based on their interaction energies. The E_{int} of RN@C_4N and FT@C_4N are −19.90 and −15.29 kcal/mol, respectively. The interaction distances (D_{int}) in RN@C_4N (H_{156}–N_{26}) and FT@C_4N (H_{161}–N_{52}) complexes are 2.52 Å and 2.56 Å, respectively. Due to the lack of terminal oxygen atoms in RN, the interaction energy is low in the RN@C_4N complex. However, the mode of interaction is completely switched to out of the cavity in the FT@C_4N complex, probably due to the larger molecular size of FT (11.23 Å). Thus, FT cannot accommodate inside the cavity. Therefore, FT interacts exohedrally with the C_4N surface in order to minimize the possible repulsion. Based on these results, the thermodynamic stability trend is as followed; DDT@C_4N > FNT@C_4N > DMDT@C_4N > RN@C_4N > FT@C_4N. The interaction energies of pesticides are compared to the interaction energies of pesticides on other surface to better judge the efficiency of C_4N. Chandiramouli et al. [32], studied the interaction of DDT on the β-antimonene nanotube. In their study, the maximum reported interaction energy of the DDT@SbNT complex is −0.208 eV (−4.84 kcal/mol). The interaction energy of the DDT@C_4N complex is nearly five-fold greater than that of DDT@SbNT complex. In another report, Yadav and coworkers investigated the interactions of chlorpyrifos and malathion pesticides with graphene oxide surface [57]. The maximum reported interaction energy is −3.01 kcal/mol. Wang et al. [58], studied the interaction between

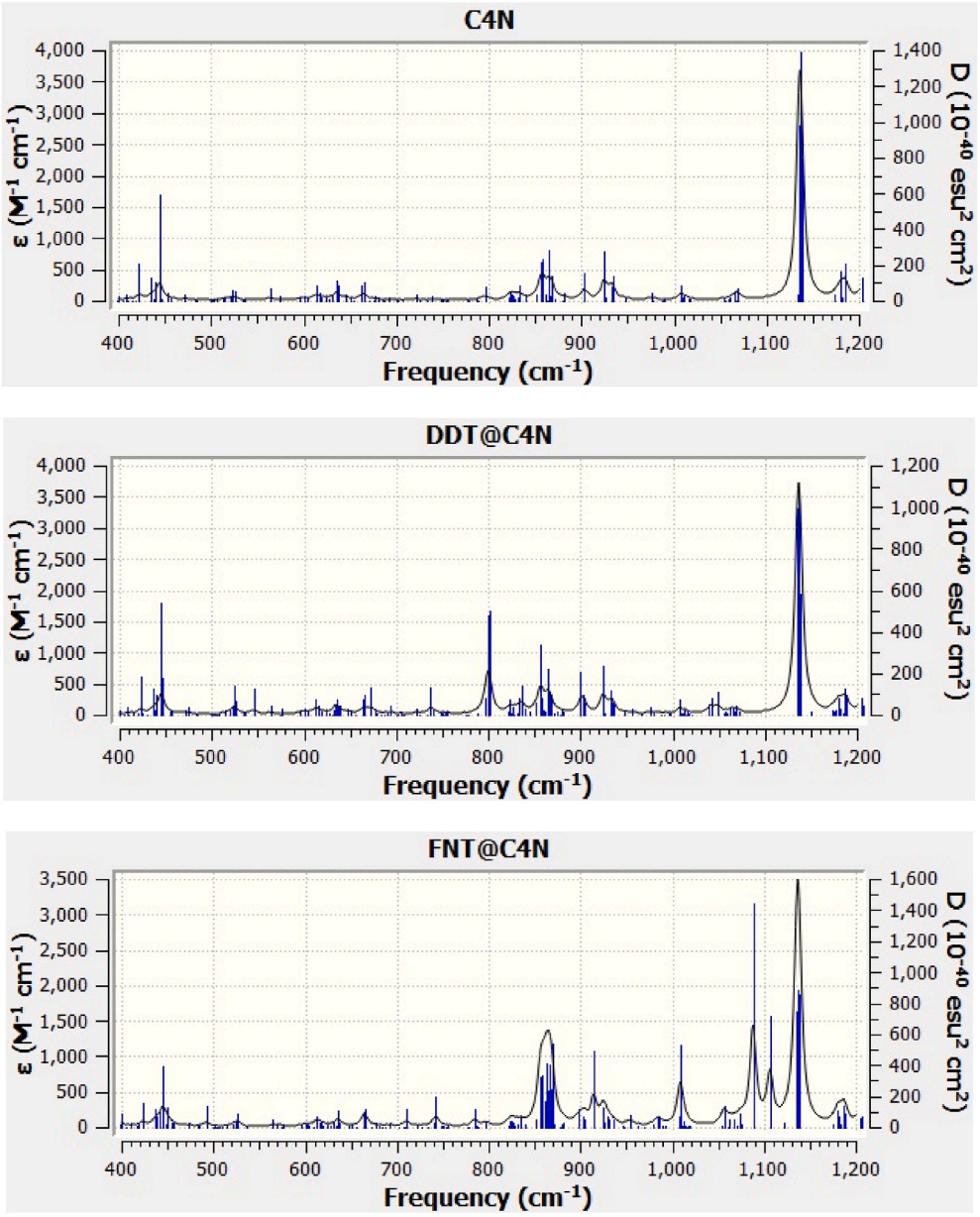

Fig. 4. IR spectra of bare and complexed C_4N.

graphene oxide and pesticides (Carbaryl, Catechol and Fluridone). The reported interaction energies for Carbaryl, Catechol and Fluoridone on graphene oxide are −19.36, −17.11 and −27.17 kcal/mol respectively. In our previous study, we reported the interaction of some toxic warfare agents i.e., A-230, A-232 & A-234 onto the graphdiyne (GDY) [59]. The interaction energies for these systems are less than 20 kcal/mol. Finally, it can be concluded that the interaction affinity of C_4N is multifold higher than most of the previously reported adsorbents.

3.2. Infrared (IR) analysis

The infrared analysis plays pivotal role in investigating the interaction mechanism [60]. Literature reveals that the noncovalent forces generate additional peaks in the neat IR region [52,61]. Herein, the IR spectra of bare and complexed C_4N are generated through harmonic approximation or vibrational analysis. These spectra of bare and complexed C_4N are given in Fig. 4. Among all the fluctuations in the region between 400 and 1000 cm^{-1}, the new peaks at 801, 858, 855, 854 and 853 cm^{-1} in the IR spectra of DDT@C_4N, FNT@C_4N, DMDT@C_4N, RN@C_4N and FT@C_4N complexes, respectively appear due to the stretching vibrations between the atoms of analytes and C_4N nanoflake.

3.3. Noncovalent interaction index (NCI) analysis

NCI analysis is performed to visualize the non-covalent interactions between C_4N and analytes. The NCI describes the strength and nature of interactions such as steric repulsion, hydrogen bonding and van der Waals forces [51]. The interactions are differentiated by different colors including, red, blue and green for steric repulsion, hydrogen bonding and van der Waals forces (dispersion), respectively. The NCI results are plotted as reduced density gradient (RDG) isosurfaces and scatter graphs of complexes. The NCI results of our reported complexes are given in Fig. 5 and Fig. S7, which clearly illustrate that the weak van der Waals interaction forces dominate in all the considered complexes. The results of NCI are well consistent with the trend of interaction energies. For instance, the more-green spikes can be observed between −0.02 and

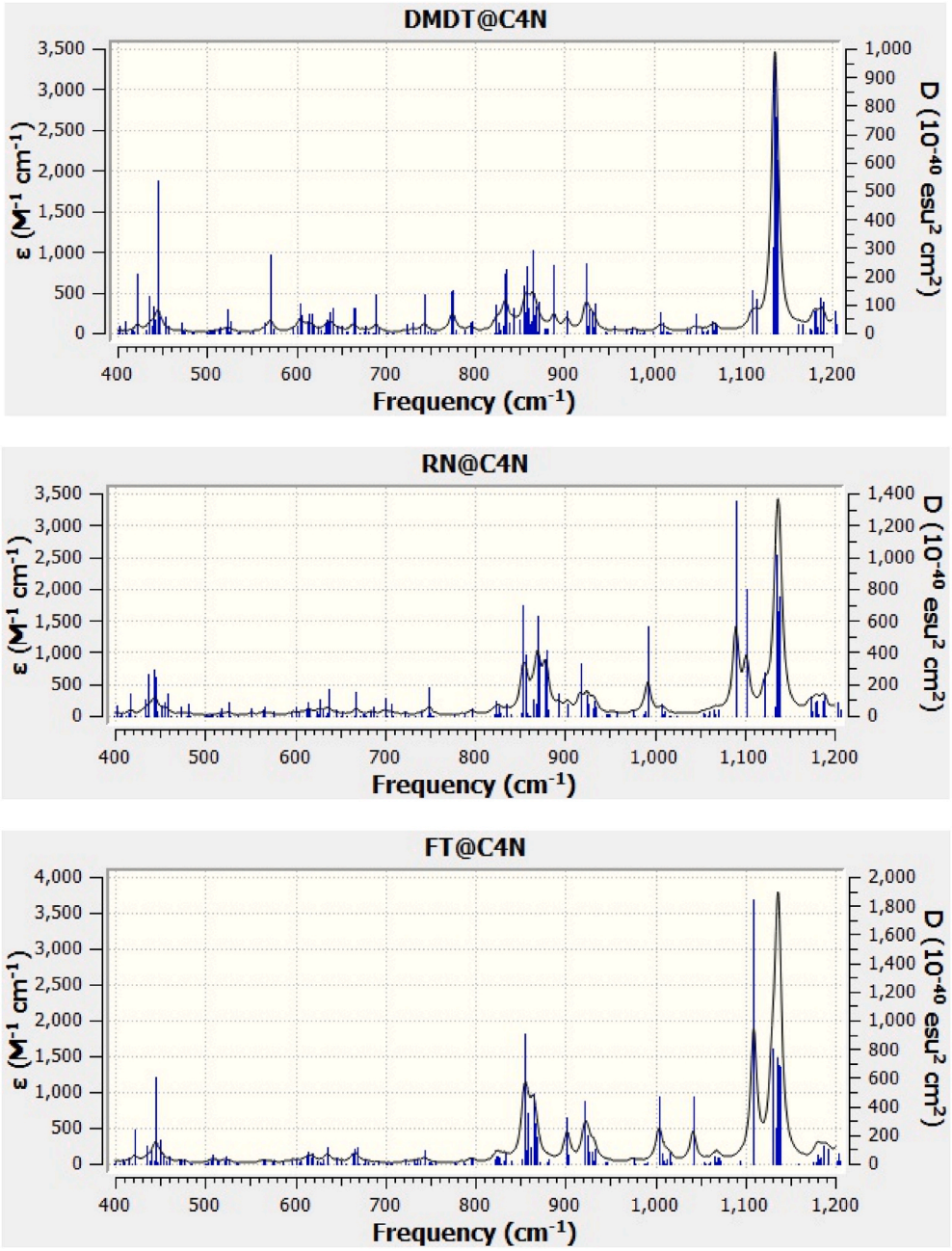

Fig. 4. (*continued*).

0.01 au of scattering RDG graphs of DDT@C_4N, FNT@C_4N and DMDT@C_4N complexes. However, the number of green spikes reduces in RN@C_4N complex which is further reduced in FT@C_4N complex. These results indicate that the contribution of dispersion forces decreases from DDT@C_4N to FT@C_4N. In the NCI results, the other contributing factor is steric repulsion which can be seen with red spikes in RDG spectra ranging from 0.01 to 0.03 au. However, the isosurfaces show that these steric repulsions are intramolecular which take place between the atoms of aromatic rings.

3.4. Quantum theory of atoms in molecules (QTAIM) analysis

The nature and strength of interaction between C_4N and pesticides (analytes) are also characterized through QTAIM analysis [61,62]. According to QTAIM analysis, the strength of the bond depends upon the electronic density (ρ) whereas bond nature depends on the Laplacian of electronic density ($\nabla^2\rho$) and the sum of electronic densities (H). The total sum of electron density (H) is the integral sum of potential energy density (V) and kinetic energy density (G) given in equation (2).

$$H = V + G \quad (2)$$

The results of QTAIM parameters are given in Table 2 while the critical points are given in Fig. 6 and Fig. S8. According to the results, FNT@C_4N and FT@C_4N complexes have the values of electron density (ρ) less than 0.1 au along with positive values of Laplacian ($\nabla^2\rho$) which depicts the presence of weak noncovalent interactions. On the other hand, the values of ρ for bond critical point (BCP) 239 and 233 for DDT@C_4N and DMDT@C_4N complexes, respectively are greater than 0.1 au along with the negative values of Laplacian ($\nabla^2\rho$) which indicate the presence of strong noncovalent interactions. Although, the RN@C_4N complex, the values of electron density for 259, 267, 303, 339 and 343 bond critical points (BCPs) are greater than 0.1 au along with the

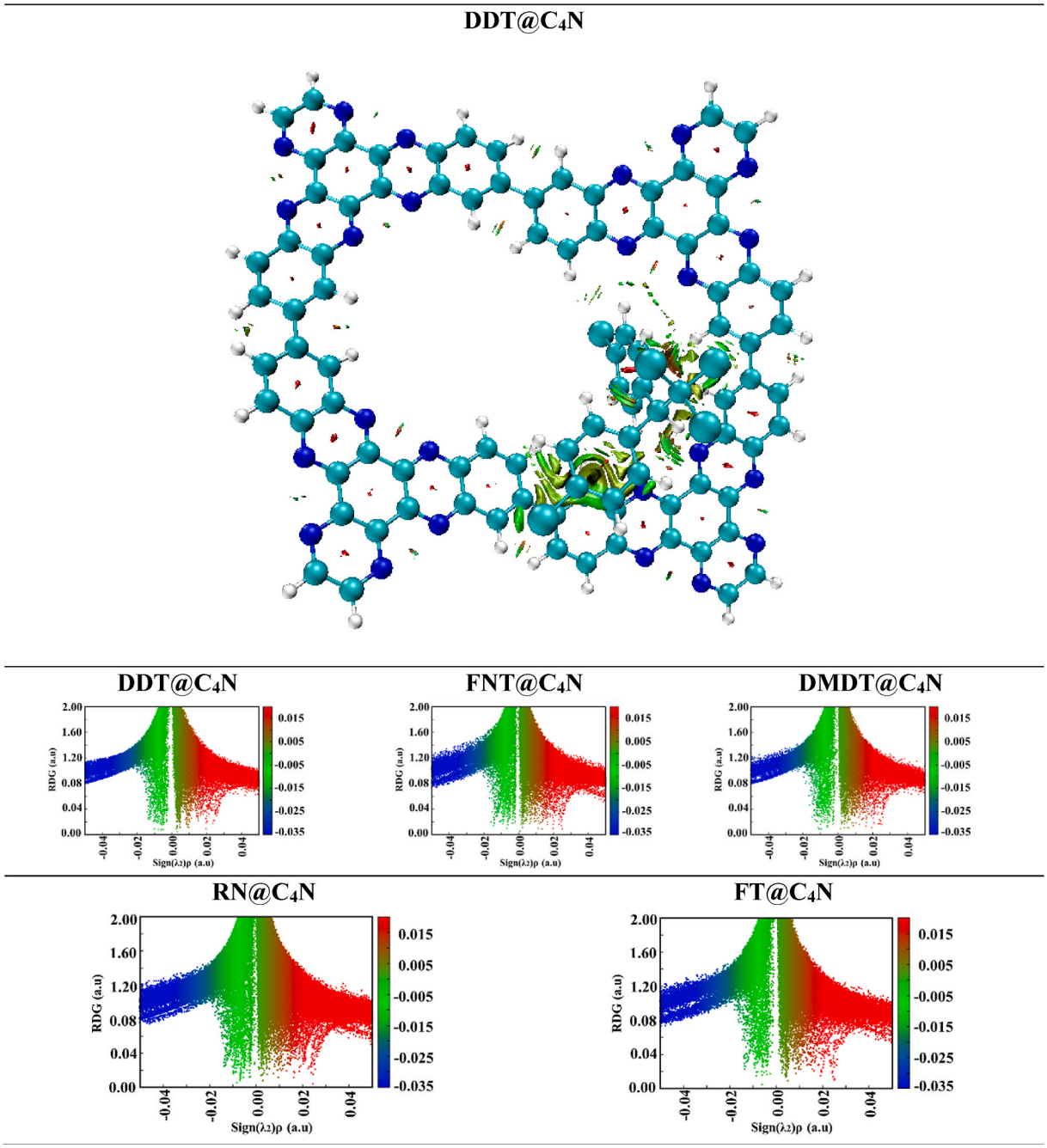

Fig. 5. NCI iso-surfaces of DDT@C_4N complex and RDG graphs of analyte@C_4N complexes.

negative values of Laplacian ($\nabla^2\rho$), but the interaction is still considered is weak noncovalent because of the larger interatomic distances (>2.5 Å) between interacting atoms. Overall, it can be postulated that the weak van der Waal forces (dispersion) dominate in the stability of complexes.

3.5. Electronic properties

After the geometric analysis, the variation in electronic parameters is computed to measure the sensitivity of C_4N towards analytes. In this regard, the energies of HOMO and LUMO orbitals along with their energy gaps (E_{gap}) are computed using ωB97XD/6-31G(d, p) level of theory. The E_{HOMO}, E_{LUMO} and respective energy gaps (E_{gap}) of bare and complexed C_4N are given in Table 3. The HOMO and LUMO energies of bare C_4N are −8.06 eV and −1.20 eV, respectively. The E_{gap} of bare C_4N is 6.85 eV. In the literature, the energy gaps between HOMO and LUMO orbitals of C_4N are 1.41 [24] and 1.97 eV [63] reported by Yu et al. Our reported E_g of C_4N is significantly different than that of the values obtained by Yu and coworkers which is due to the different choice of the density functional level of theory. For example, in the previous studies, the author calculated the results at the B3LYP/6-31G(d, p) level whereas, our results are obtained at the long range ωB97XD/6-31G(d, p) DFT level. For comparison, we have also calculated the E_g of bare C_4N at the B3LYP/6-31G(d, p) which is about 2.09 eV. At this point, we can assume that the accuracy of the results depends upon the selection of suitable functional. Furthermore, from the results, it is revealed that the energy gap of C_4N decreases upon complexation with analytes which ultimately indicates the change in the conductivity. The observed E_{gap} in DDT@C_4N, FNT@C_4N, DMDT@C_4N, RN@C_4N and FT@C_4N complexes are 6.75, 6.55, 6.30, 6.69 and 6.74 eV, respectively. The decrease in the

Table 2
QTAIM results of DDT@C_4N FNT@C_4N, DMDT@C_4N, RN@C_4N and FT@C_4N complexes. Where BCPs (bond critical points), ρ (electron density), $\nabla^2\rho$ (Laplacian electron density), G (kinetic energy density), V (potential energy density) and H (sum of electron density).

BCPs	Analyte ··· C_4N	ρ	$\nabla^2\rho$	G	V	H
DDT@C_4N						
215	H_{161}–N_{118}	0.0066	0.023	0.0046	−0.0035	0.00111
219	H_{161}–N_{120}	0.0114	0.031	0.0073	−0.0069	0.00040
229	C_{150}–H_{124}	0.0046	0.014	0.0028	−0.0020	0.00081
237	Cl_{138}–H_{131}	0.0067	0.024	0.0046	−0.0032	0.00145
239	C_{151}–C_{14}	0.3561	−0.947	0.3617	−0.9603	−0.59859
248	C_{140}–H_{126}	0.0033	0.011	0.0020	−0.0013	0.00068
249	C_{137}–H_{157}	0.0111	0.042	0.0085	−0.0065	0.00198
262	C_{148}–H_{131}	0.0078	0.023	0.0049	−0.0040	0.00101
285	H_{156}–N_{26}	0.0075	0.022	0.0049	−0.0042	0.00069
293	H_{159}–N_{26}	0.0082	0.028	0.0059	−0.0046	0.00119
307	H_{159}–N_{24}	0.0130	0.034	0.0084	−0.0081	0.00029
315	C_{147}–N_{24}	0.0053	0.016	0.0035	−0.0028	0.00065
320	C_{149}–H_{30}	0.0049	0.016	0.0032	−0.0023	0.00077
343	C_{155}–C_{46}	0.0031	0.009	0.0018	−0.0014	0.00046
373	Cl_{141}–C_{41}	0.0063	0.019	0.0039	−0.0029	0.00096
FNT@C_4N						
213	H_{157}–N_{118}	0.0092	0.029	0.0064	−0.0053	0.00105
238	O_{140}–H_{122}	0.0097	0.030	0.0072	−0.0068	0.00042
250	C_{146}–H_{124}	0.0064	0.020	0.0040	−0.0028	0.00115
251	O_{141}–H_{129}	0.0050	0.018	0.0037	−0.0029	0.00083
257	O_{141}–H_{122}	0.0055	0.021	0.0043	−0.0037	0.00091
257	O_{140}–H_{129}	0.0055	0.021	0.0043	−0.0037	0.00091
259	H_{161}–H_{92}	0.0048	0.020	0.0037	−0.0024	0.00131
268	O_{139}–H_{92}	0.0055	0.020	0.0044	−0.0036	0.00076
279	H_{163}–N_{86}	0.0068	0.023	0.0048	−0.0037	0.00103
293	H_{163}–N_{88}	0.0077	0.023	0.0050	−0.0043	0.00073
320	C_{147}–H_{61}	0.0022	0.007	0.0013	−0.0009	0.00044
322	C_{147}–H_{60}	0.0021	0.007	0.0013	−0.0009	0.00043
326	S_{135}–H_{60}	0.0033	0.009	0.0018	−0.0011	0.00061
340	H_{160}–H_{60}	0.0035	0.012	0.0023	−0.0014	0.00082
352	H_{158}–H_{58}	0.0033	0.012	0.0022	−0.0014	0.00080
359	H_{159}–N_{56}	0.0093	0.028	0.0063	−0.0055	0.00081
362	H_{159}–N_{54}	0.0092	0.028	0.0062	−0.0054	0.00084
DMDT@C_4N						
203	C_{149}–C_{101}	0.0063	0.019	0.0040	−0.0031	0.00092
216	H_{162}–C_{103}	0.0081	0.027	0.0056	−0.0043	0.00130
233	H_{169}–N_{24}	0.2861	−1.049	0.0389	−0.3401	−0.30118
248	Cl_{139}–C_{110}	0.0028	0.009	0.0017	−0.0012	0.00048
249	H_{159}–N_{120}	0.0154	0.042	0.0102	−0.0099	0.00035
254	H_{158}–C_{106}	0.0072	0.022	0.0045	−0.0037	0.00106
268	Cl_{139}–H_{94}	0.0023	0.008	0.0014	−0.0009	0.00046
270	H_{163}–H_{124}	0.0057	0.021	0.0039	−0.0026	0.00133
298	O_{140}–H_{131}	0.0097	0.030	0.0071	−0.0067	0.00039
323	H_{169}–N_{26}	0.0099	0.031	0.0068	−0.0059	0.00087
330	Cl_{137}–H_{136}	0.0000	0.000	0.0000	−0.0000	0.00000
341	H_{167}–H_{30}	0.0031	0.011	0.0019	−0.0012	0.00073
RN@C_4N						
199	Cl_{134}–C_{40}	0.0054	0.017	0.0034	−0.0025	0.00092
206	Cl_{135}–N_{54}	0.0055	0.017	0.0036	−0.0029	0.00075
207	Cl_{135}–N_{54}	0.0028	0.010	0.0021	−0.0015	0.00054
234	C_{143}–C_{42}	0.0067	0.019	0.0039	−0.0031	0.00082
259	O_{140}–H_{30}	0.3432	−1.041	0.2974	−0.8551	−0.55777
267	C_{148}–N_{24}	0.2783	−0.725	0.0655	−0.3124	−0.24697
283	H_{156}–N_{26}	0.0244	0.187	0.0377	−0.0285	0.00919
303	O_{139}–H_{127}	0.3024	−0.828	0.0853	−0.3778	−0.29246
305	S_{136}–H_{122}	0.0011	0.003	0.0006	−0.0004	0.00024
309	Cl_{133}–C_{110}	0.0164	0.123	0.0236	−0.0164	0.00724
339	H_{152}–N_{118}	0.3283	−0.931	0.1145	−0.4619	−0.34744
343	H_{152}–N_{116}	0.3238	−0.902	0.1115	−0.4487	−0.33720
FT@C_4N						
178	H_{161}–N_{52}	0.0098	0.032	0.0069	−0.0059	0.00103
188	H_{155}–N_{52}	0.0026	0.009	0.0018	−0.0012	0.00059
190	H_{161}–N_{53}	0.0091	0.026	0.0060	−0.0054	0.00066
206	C_{148}–N_{53}	0.0064	0.020	0.0042	−0.0034	0.00081
244	C_{147}–C_{43}	0.0074	0.021	0.0045	−0.0035	0.00095
274	S_{138}–H_{64}	0.0089	0.026	0.0055	−0.0043	0.00116
291	S_{138}–C_{79}	0.0042	0.012	0.0023	−0.0017	0.00066
301	H_{164}–C_{80}	0.0061	0.020	0.0039	−0.0028	0.00110
307	H_{163}–C_{75}	0.0198	0.156	0.0303	−0.0217	0.00864

E_g of C_4N upon complexation with pesticide molecules indicate the lowering of semiconducting properties. The trend of semiconducting nature of complexes is as follow: DDT@C_4N > FT@C_4N > RN@C_4N > FNT@C_4N > DMDT@C_4N. The lowering of E_{gap} of C_4N is due to the shifting of LUMO (virtual) orbitals toward Fermi energy level upon complexation. The shifting of virtual orbitals towards Fermi energy level can be observed from the density of state (DOS) spectra. The DOS spectra of bare and DDT@C_4N are given in Fig. 7 whereas, DOS spectra for FNT@C_4N, DMDT@C_4N, RN@C_4N and FT@C_4N complexes are given in the supplementary information (Fig. S9 and Fig. S10). The DOS spectra illustrate that the more pronounced shifts of orbitals are seen in the DMDT@C_4N complex, where the virtual orbital shifts from −1.20 eV (bare C_4N) to −1.31 eV in DMDT@C_4N complex. Similarly, the virtual orbitals of FNT@C_4N, DMDT@C_4N, RN@C_4N and FT@C_4N complexes are shifted to −1.34, −1.24, −1.34 and −1.24 eV. Due to the shifting of virtual orbitals towards the Fermi level, the energy gaps of complexes reduce which results the increase in conductivity of the systems. Thereby, the transfer of charge takes place between interacting species. To measure the amount of charge transfer upon complexation, the CHELPG charge transfer [64,65] analysis is performed. The amount of CHELPG charge transfer in DDT@C_4N, FNT@C_4N, DMDT@C_4N, RN@C_4N and FT@C_4N complexes is −0.22, −0.20, −0.15, −0.13 and −0.15 e−, respectively.

3.6. Electron density differences (EDD)

Electron density difference (EDD) analysis is performed to visualize the charge separation between analytes and C_4N upon complexation. The EDD isosurface of DDT@C_4N is given in Fig. 8, however, the isosurfaces of FNT@C_4N, DMDT@C_4N, RN@C_4N and FT@C_4N are displayed in the supplementary information (Fig. S11). In EDD, the electronic density is differentiated by two colors such as red and blue which indicate the decrease and increase of electron density, respectively. Fig. 8 shows the large electronic density on the DDT molecule which is very much consistent with the CHELPG charge transfer analysis. The electronic density shifts from N_{120} and N_{118} of C_4N to the H_{161} of DDT. Moreover, the chlorine atom of DDT also fetches the π-electrons of the aromatic ring from the other side of C_4N. However, the isosurface of the FNT@C_4N complex depicts the equal distribution of charge density on all the atoms of the complex because the analyte (FNT) is equally interacting from all the sides of the surface. In addition, the more electron density (blue color) is located between the H_{92} of C_4N and O_{139} of FNT (Fig. 8) which attributes the significant donation of electrons that takes place through this particular site of interaction. Similarly, the electronic densities of DMDT@C_4N, RN@C_4N and FT@C_4N complexes are more localized between the atoms where interactions are maximum (see Fig. S11).

3.7. Charge decomposition (CDA) analysis

Charge decomposition (CDA) analysis is performed to analyze the relative strength of donor-accepter interactions in terms of charge transfer [66,67]. CDA analysis is simulated to determine the donation and back donation of charges between C_4N (donor) and analytes (accepter). The results of CDA for analytes@C_4N complexes are summarized in Table 4. From the results of donation in complexes, one can infer that the significant charge is transferred from C_4N to RN in the RN@C_4N complex. However, the back donation, the donation of charges from analyte (FNT) to C_4N, is more pronounced in the FNT@C_4N complex which might be due to the interaction between the electron rich oxygen atoms of FNT and electron deficient hydrogen atoms of C_4N. In addition, the value of charge residual in the FNT@C_4N complex is significantly high (−0.623 e^-). Furthermore, the negative value also indicates that the back donation or charge transfer from analyte (FNT) to surface (C_4N) dominates in the complex (FNT@C_4N). Expectedly, the back donation of charges in the DDT@C_4N complex is negligible which

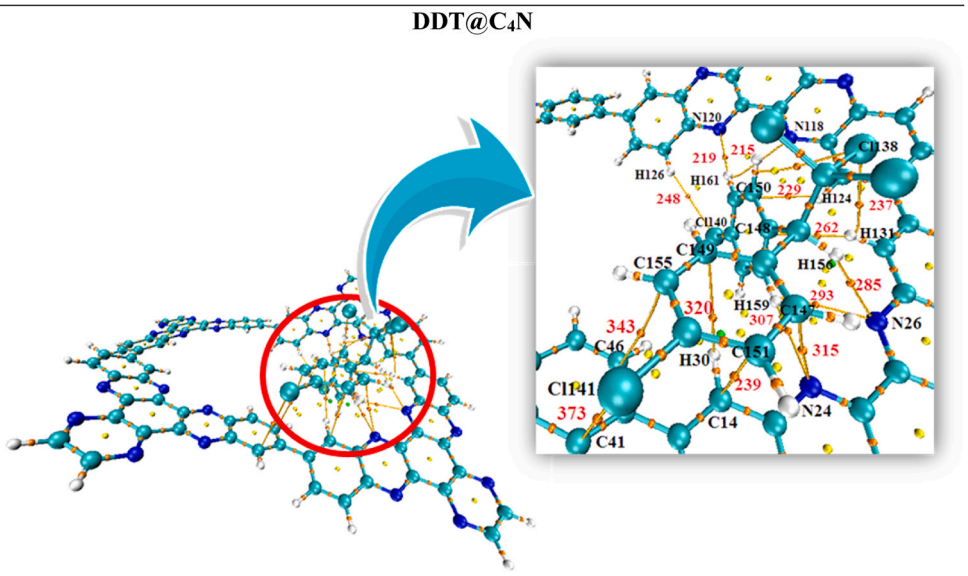

Fig. 6. QTAIM analysis results of DDT@C_4N complex.

Table 3
The electronic parameters including HOMO-LUMO energies, Energy gap, CHELPG charge transfer and UV–Vis results of bare C_4N and analyte@C_4N.

Properties	C_4N	DDT@C_4N	FNT@C_4N	DMDT@C_4N	RN@C_4N	FT@C_4N
HOMO	−8.06	−8.06	−7.89	−7.54	−8.03	−7.98
LUMO	−1.20	−1.31	−1.34	−1.24	−1.34	−1.24
E_g	6.85	6.75	6.55	6.30	6.69	6.74
CHELPG	–	−0.22	−0.20	−0.15	−0.13	−0.15

Note: The unit of HOMO, LUMO and Eg is eV while for CHELPG is e−.

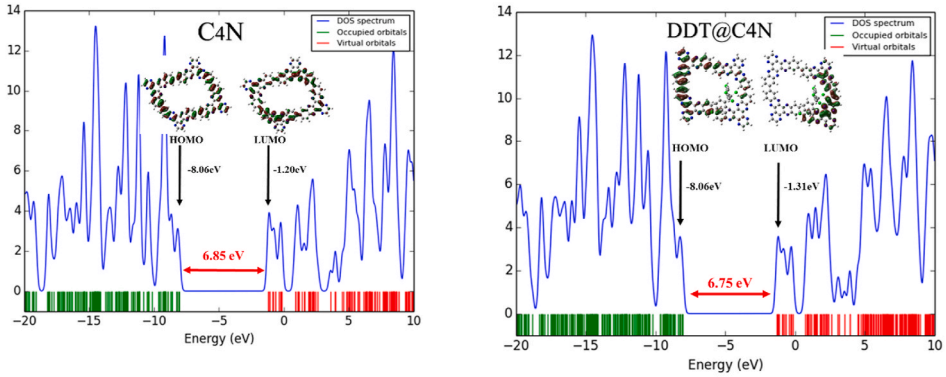

Fig. 7. DOS spectra of bare C_4N and DDT@C_4N complex (at energy x-axis, green vertical lines show occupied orbitals and red show virtual orbitals).

is 0.001 e^-. Thus, the significant charge transferred is noticed in the DDT@C_4N complex. Moreover, the value of repulsion plays an important role to explain the distribution of charge densities between the donor (C_4N) and accepter (analyte). The repulsion between the similar charges in DDT@C_4N, FNT@C_4N, DMDT@C_4N, RN@C_4N and FT@C_4N complexes are −0.023, 0.355 e^-, −0.070, −0.033 e^- and −0.035 e^-, respectively. The positive value of repulsion illustrates that the charge density is accumulated within the interaction region whereas, the negative value depicts that charge density is moving away from the interaction region. For example, the HOMO orbitals of FNT@C_4N (Fig. 8) are located in the region where interaction dominates between the oxygen of para-nitro group FNT and hydrogen of C_4N. Thus, the value of repulsion is positive in the FNT@C_4N complex. On the other hand, the electron rich orbitals are located away from the interaction region thus, the HOMO orbitals of DDT@C_4N, DMDT@C_4N, RN@C_4N and FT@C_4N complexes are located away from the interacting regions.

4. Conclusion

Potential of C_4N surface as electrochemical sensor for pesticides is

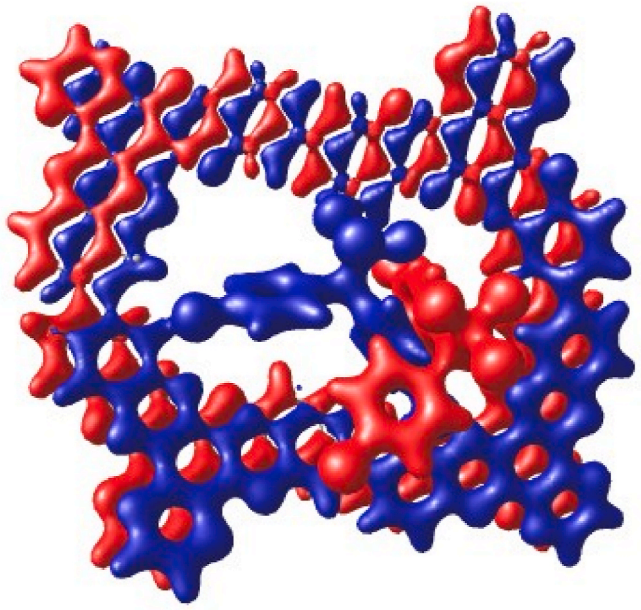

Fig. 8. EDD isosurface of DDT@C_4N complex representing the charge density distribution wit the iso-value of 0.004 au.

Table 4
CDA results including donation (d), back donation (b), residual (d-b) and repulsion (r). The unit of the values in the table is electron (e^-).

Complex	Donation (d)	Back donation(b)	Residual (d-b)	Repulsion (r)
DDT@C_4N	0.034	0.001	0.034	−0.023
FNT@C_4N	0.077	0.701	−0.623	0.355
DMDT@C_4N	0.039	0.026	0.014	−0.070
RN@C_4N	0.254	−0.15	0.407	−0.033
FT@C_4N	0.019	0.008	0.011	−0.035

explored through DFT calculations. Based on the interaction strength and adsorption structure, it is found that C_4N is a selective sensor of toxic molecules. Moreover, the interaction of pesticides causes significant changes in the electronic and structural behavior of C_4N because these analytes can easily accommodate inside the porous cavity of C_4N. Thus, the interaction between C_4N and FNT or RN is maximum. The interaction energies of DDT@C_4N (−24.37 kcal/mol) and FNT@C_4N (−21.79 kcal/mol) are higher than DMDT@C_4N (−21.43 kcal/mol), RN@C_4N (−19.90 kcal/mol) and FT@C_4N (−15.29 kcal/mol). Moreover, the HOMO-LUMO gaps are significantly decreased upon complexation with pesticides, especially in the DMDT@C_4N complex. Thus, variations in electronic properties of C_4N are quantified through HOMO-LUMO charge transfer and CHELPG charge transfer analysis. According to these electronic parameters, the trend of sensitivity of complexes is a follow: DDT@C_4N > FNT@C_4N > DMDT@C_4N > FT@C_4N > RN@C_4N. This order of sensitivity is much consistent with the energetic analysis. Finally, from the compendium of this study, we may envisage that C_4N can be a potential candidate for applications in the sensor devices to detect poisonous molecules.

Declaration of competing interest

The authors declare that they have no known competing financial interests or personal relationships that could have appeared to influence the work reported in this paper.

Acknowledgements

The authors acknowledge the Higher Education Commission of Pakistan and COMSATS University, Abbottabad Campus for financial support.

Appendix A. Supplementary data

Supplementary data to this article can be found online at https://doi.org/10.1016/j.jpcs.2021.110345.

References

[1] L. Ge, X. Mu, G. Tian, Q. Huang, J. Ahmed, Z. Hu, Current applications of gas sensor based on 2-D nanomaterial: a mini review, Front. Chem. 7 (2019) 839, https://doi.org/10.3389/fchem.2019.00839.
[2] M.A.H. Khan, M. V Rao, Q. Li, Recent Advances in Electrochemical Sensors for Detecting Toxic Gases: NO_2, SO_2 and H_2S, Sensors (Basel), vol. 19, 2019, p. 905, https://doi.org/10.3390/s19040905.
[3] D. Gregor-Svetec, Chapter 8-intelligent packaging, in: M.Â.P.R. Cerqueira, J. M. Lagaron, L.M. Pastrana Castro, Vicente de Oliveira Soares (Eds.), Micro Nano Technol., Elsevier, 2018, pp. 203–247, https://doi.org/10.1016/B978-0-323-51271-8.00008-5. A.A.M.B.T.-N. for F.P.
[4] S. Gupta Chatterjee, S. Chatterjee, A.K. Ray, A.K. Chakraborty, Graphene–metal oxide nanohybrids for toxic gas sensor: a review,, Sensor. Actuator. B Chem. 221 (2015) 1170–1181, https://doi.org/10.1016/j.snb.2015.07.070.
[5] M. Yar, K. Ayub, Expanding the horizons of covalent organic frameworks to electrochemical sensors; A case study of CTF-FUM, Microporous Mesoporous Mater. 300 (2020) 110146, https://doi.org/10.1016/j.micromeso.2020.110146.
[6] H. Yuan, N. Li, J. Linghu, J. Dong, Y. Wang, A. Karmakar, J. Yuan, M. Li, P.J. S. Buenconsejo, G. Liu, H. Cai, S.J. Pennycook, N. Singh, D. Zhao, Chip-level integration of covalent organic frameworks for trace benzene sensing, ACS Sens. 5 (2020) 1474–1481, https://doi.org/10.1021/acssensors.0c00495.
[7] V. Pentyala, P. Davydovskaya, M. Ade, R. Pohle, G. Urban, Metal–organic frameworks for alcohol gas sensor, Sensor. Actuator. B Chem. 222 (2016) 904–909, https://doi.org/10.1016/j.snb.2015.09.014.
[8] X. Wang, S. Li, L. Xie, X. Li, D. Lin, Z. Zhu, Low-temperature and highly sensitivity H2S gas sensor based on ZnO/CuO composite derived from bimetal metal-organic frameworks, Ceram. Int. 46 (2020) 15858–15866, https://doi.org/10.1016/j.ceramint.2020.03.133.
[9] K. Tao, X. Han, Q. Yin, D. Wang, L. Han, L. Chen, Metal-organic frameworks-derived porous In2O3 hollow nanorod for high-performance ethanol gas sensor, Chemistry 2 (2017) 10918–10925, https://doi.org/10.1002/slct.201701752.
[10] A. Dey, Semiconductor metal oxide gas sensors: a review,, Mater. Sci. Eng. B 229 (2018) 206–217, https://doi.org/10.1016/j.mseb.2017.12.036.
[11] C.A. Papadopoulos, D.S. Vlachos, J.N. Avaritsiotis, Comparative study of various metal-oxide-based gas-sensor architectures, Sensor. Actuator. B Chem. 32 (1996) 61–69, https://doi.org/10.1016/0925-4005(96)80110-9.
[12] H.J. Yoon, D.H. Jun, J.H. Yang, Z. Zhou, S.S. Yang, M.M.-C. Cheng, Carbon dioxide gas sensor using a graphene sheet, Sensor. Actuator. B Chem. 157 (2011) 310–313, https://doi.org/10.1016/j.snb.2011.03.035.
[13] A. Satsuma, K. Shimizu, T. Hattori, H. Nishiyama, S. Kakimoto, S. Sugaya, H. Yokoi, Polytungstate clusters on zirconia as a sensing material for a selective ammonia gas sensor, Sensor. Actuator. B Chem. 123 (2007) 757–762, https://doi.org/10.1016/j.snb.2006.10.011.
[14] A.S. Rad, K. Ayub, Enhancement in hydrogen molecule adsorption on B12N12 nano-cluster by decoration of nickel, Int. J. Hydrogen Energy 41 (2016) 22182–22191, https://doi.org/10.1016/j.ijhydene.2016.08.158.
[15] G. Singh, A. Choudhary, D. Haranath, A.G. Joshi, N. Singh, S. Singh, R. Pasricha, ZnO decorated luminescent graphene as a potential gas sensor at room temperature, Carbon N. Y. 50 (2012) 385–394, https://doi.org/10.1016/j.carbon.2011.08.050.
[16] R. Zou, G. He, K. Xu, Q. Liu, Z. Zhang, J. Hu, ZnO nanorods on reduced graphene sheets with excellent field emission, gas sensor and photocatalytic properties, J. Mater. Chem. 1 (2013) 8445–8452, https://doi.org/10.1039/C3TA11490B.
[17] P.F. Greenwood, K.R. Arouri, G.A. Logan, R.E. Summons, Abundance and geochemical significance of C2n dialkylalkanes and highly branched C3n alkanes in diverse Meso- and Neoproterozoic sediments, Org. Geochem. 35 (2004) 331–346, https://doi.org/10.1016/j.orggeochem.2003.10.013.
[18] H. Cui, K. Zheng, Y. Zhang, H. Ye, X. Chen, Superior selectivity and sensitivity of C3N sensor in probing toxic gases NO2 and SO2, IEEE Electron. Device Lett. 39 (2018) 284–287, https://doi.org/10.1109/LED.2017.2787788.
[19] M. Yar, M.A. Hashmi, A. Khan, K. Ayub, Carbon nitride 2-D surface as a highly selective electrochemical sensor for V-series nerve agents, J. Mol. Liq. 311 (2020) 113357, https://doi.org/10.1016/j.molliq.2020.113357.
[20] M. Yar, M.A. Hashmi, K. Ayub, Nitrogenated holey graphene (C2N) surface as highly selective electrochemical sensor for ammonia, J. Mol. Liq. (2019) 111929, https://doi.org/10.1016/j.molliq.2019.111929.
[21] K. Bhattacharyya, S.M. Pratik, A. Datta, Controlled pore sizes in monolayer C2N act as ultrasensitive probes for detection of gaseous pollutants (HF, HCN, and H2S), J. Phys. Chem. C 122 (2018) 2248–2258, https://doi.org/10.1021/acs.jpcc.7b11963.

[22] X. Li, T. Guo, L. Zhu, C. Ling, Q. Xue, W. Xing, Charge-modulated CO2 capture of C3N nanosheet: insights from DFT calculations, Chem. Eng. J. 338 (2018) 92–98, https://doi.org/10.1016/j.cej.2017.12.113.

[23] A. Bafekry, M. Ghergherehchi, S. Farjami Shayesteh, F.M. Peeters, Adsorption of molecules on C3N nanosheet: a first-principles calculations, Chem. Phys. 526 (2019) 110442, https://doi.org/10.1016/j.chemphys.2019.110442.

[24] Y. Li, C. Mo, J. Li, D. Yu, Pyrazine–nitrogen–rich exfoliated C4N nanosheets as efficient metal–free polymeric catalysts for oxygen reduction reaction, J. Energy Chem. 49 (2020) 243–247, https://doi.org/10.1016/j.jechem.2020.02.046.

[25] D. Pimentel, Amounts of pesticides reaching target pests: environmental impacts and ethics, J. Agric. Environ. Ethics 8 (1995) 17–29, https://doi.org/10.1007/BF02286399.

[26] A. Sabarwal, K. Kumar, R.P. Singh, Hazardous effects of chemical pesticides on human health-Cancer and other associated disorders, Environ. Toxicol. Pharmacol. 63 (2018) 103–114, https://doi.org/10.1016/j.etap.2018.08.018.

[27] A.M. Soto, K.L. Chung, C. Sonnenschein, The pesticides endosulfan, toxaphene, and dieldrin have estrogenic effects on human estrogen-sensitive cells., Environ, Health Perspect. 102 (1994) 380–383, https://doi.org/10.1289/ehp.94102380.

[28] I.A. al-Saleh, Pesticides: a review article, J. Environ. Pathol. Toxicol. Oncol. Off. Organ Int. Soc. Environ. Toxicol. Cancer 13 (1994) 151–161.

[29] T. Galloway, R. Handy, Immunotoxicity of organophosphorous pesticides, Ecotoxicology 12 (2003) 345–363, https://doi.org/10.1023/a:1022579416322.

[30] F.P. Carvalho, Pesticides, environment, and food safety, Food Energy Secur 6 (2017) 48–60. https://doi.org/10.1002/fes3.108.

[31] P. Nicolopoulou-Stamati, S. Maipas, C. Kotampasi, P. Stamatis, L. Hens, Chemical pesticides and human health: the urgent need for a new concept in agriculture, Front. Public Heal 4 (2016) 148, https://doi.org/10.3389/fpubh.2016.00148.

[32] R. Bhuvaneswari, V. Nagarajan, R. Chandiramouli, Sensing studies of DDT and Toxaphene molecules using chemi-resistive β-antimonene nanotubes based on first-principles insights, Chem. Phys. Lett. 757 (2020), 137895, https://doi.org/10.1016/j.cplett.2020.137895.

[33] M.C.R. Alavanja, J.A. Hoppin, F. Kamel, Health effects of chronic pesticide exposure: cancer and neurotoxicity, Annu. Rev. Publ. Health 25 (2004) 155–197, https://doi.org/10.1146/annurev.publhealth.25.101802.123020.

[34] V. Turusov, V. Rakitsky, L. Tomatis, Dichlorodiphenyltrichloroethane (DDT): ubiquity, persistence, and risks, Environ. Health Perspect. 110 (2002) 125–128, https://doi.org/10.1289/ehp.02110125.

[35] B.A. Cohn, M.S. Wolff, P.M. Cirillo, R.I. Sholtz, DDT and breast cancer in young women: new data on the significance of age at exposure, environ, Health Perspect. 115 (2007) 1406–1414, https://doi.org/10.1289/ehp.10260.

[36] M. Farghaly, S. El-Maghraby, Investigation of chronic toxicity of 14C-fenitrothion and its degradation products on stored soybeans, Environ. Toxicol. Pharmacol. 27 (2009) 1–6, https://doi.org/10.1016/j.etap.2008.08.005.

[37] A. Mejri, A. Mars, H. Elfil, A.H. Hamzaoui, Reduced graphene oxide nanosheets modified with nickel disulfide and curcumin nanoparticles for non-enzymatic electrochemical sensing of methyl parathion and 4-nitrophenol, Mikrochim. Acta 186 (2019) 704, https://doi.org/10.1007/s00604-019-3853-3.

[38] X. Huang, J. Liu, Z. Pi, Z. Yu, Qualitative and quantitative analysis of organophosphorus pesticide residues using temperature modulated SnO(2) gas sensor, Talanta 64 (2004) 538–545, https://doi.org/10.1016/j.talanta.2004.03.022.

[39] Z. Jing, J. Zhan, Fabrication, Gas-Sensing Properties, Of porous ZnO nanoplates, adv, Mater 20 (2008) 4547–4551, https://doi.org/10.1002/adma.200800243.

[40] S. Boulanouar, S. Mezzache, A. Combès, V. Pichon, Molecularly imprinted polymers for the determination of organophosphorus pesticides in complex samples, Talanta 176 (2018) 465–478, https://doi.org/10.1016/j.talanta.2017.08.067.

[41] R. Bhuvaneswari, V. Nagarajan, R. Chandiramouli, Molecular interaction of oxytetracycline and sulfapyridine on blue phosphorene nanotubes: a first-principles insight, Phys. Lett. 394 (2021) 127198, https://doi.org/10.1016/j.physleta.2021.127198.

[42] J. Princy Maria, R. Bhuvaneswari, V. Nagarajan, R. Chandiramouli, Kagome phosphorene molecular device for sensing chloropicrin and phosgene – a first-principles study, Chem. Phys. Lett. 771 (2021) 138472, https://doi.org/10.1016/j.cplett.2021.138472.

[43] V. Nagarajan, R. Chandiramouli, Interaction studies of glycine, acetate and methylamine on β-tellurene nanoribbon – a first-principles analysis, J. Mol. Graph. Model. 105 (2021) 107895, https://doi.org/10.1016/j.jmgm.2021.107895.

[44] R. Bhuvaneswari, V. Nagarajan, R. Chandiramouli, Interaction studies of diclofenac and ibuprofen molecules on armchair bismuthene nanotubes: a first-principles study, Chem. Phys. 546 (2021) 111169, https://doi.org/10.1016/j.chemphys.2021.111169.

[45] R. Bhuvaneswari, V. Nagarajan, R. Chandiramouli, Interaction studies of nitrotoluene and toluidine molecules on novel square-octagon arsenene nanotubes based on DFT method, J. Mol. Liq. 325 (2021) 115260, https://doi.org/10.1016/j.molliq.2020.115260.

[46] J. Xu, J. Mahmood, Y. Dou, S. Dou, F. Li, L. Dai, J. Baek, 2D frameworks of C 2 N and C 3 N as new anode materials for lithium-ion batteries, Adv. Mater. 29 (2017) 1702007, https://doi.org/10.1002/adma.201702007.

[47] L. Li, X. Kong, O. Leenaerts, X. Chen, B. Sanyal, F.M. Peeters, Carbon-rich carbon nitride monolayers with Dirac cones: dumbbell C4N, Carbon N. Y. 118 (2017) 285–290, https://doi.org/10.1016/j.carbon.2017.03.045.

[48] J.R. Frisch, J.T. M, G.W. Schlegel, H.B. Scuseria, G.E. Robb, M.A. Cheeseman, G. A. Scalmani, G. Barone, V. Mennucci, B. Petersson, Gaussian 09, Rev. D. 0.1, Gaussian, Inc, Wallingford, CT, 2013 n.d.

[49] J. Dennington, Roy; keith, todd; millam, GaussView 5.0. Shawnee Mission KS 5 (2009).

[50] Z. Jia, H. Pang, H. Li, X. Wang, A density functional theory study on complexation processes and intermolecular interactions of triptycene-derived oxacalixarenes, Theor. Chem. Acc 138 (2019) 113, https://doi.org/10.1007/s00214-019-2502-6.

[51] S. Khan, H. Sajid, K. Ayub, T. Mahmood, Adsorption behaviour of chronic blistering agents on graphdiyne; excellent correlation among SAPT, reduced density gradient (RDG) and QTAIM analyses, J. Mol. Liq. 316 (2020) 113860, https://doi.org/10.1016/j.molliq.2020.113860.

[52] M. Asif, H. Sajid, F. Ullah, S. Khan, K. Ayub, M. Amjad Gilani, M. Arshad, M. Salim Akhter, T. Mahmood, Quantum chemical study on sensing of NH3, NF3, NCl3 and NBr3 by using cyclic tetrapyrrole, Comput, Theor. Chem. 1199 (2021) 113221, https://doi.org/10.1016/j.comptc.2021.113221.

[53] N. Mardirossian, M. Head-Gordon, How accurate are the Minnesota density functionals for noncovalent interactions, isomerization energies, thermochemistry, and barrier heights involving molecules composed of main-group elements? J. Chem. Theor. Comput. 12 (2016) 4303–4325, https://doi.org/10.1021/acs.jctc.6b00637.

[54] S. Grimme, Density functional theory with London dispersion corrections, Wiley Interdiscip. Rev. Comput. Mol. Sci. 1 (2011) 211–228, https://doi.org/10.1002/wcms.30.

[55] T. Lu, F. Chen, Multiwfn: a multifunctional wavefunction analyzer,, J. Comput. Chem. 33 (2012) 580–592, https://doi.org/10.1002/jcc.22885.

[56] N.M. O'boyle, A.L. Tenderholt, K.M. Langner, cclib: a library for package-independent computational chemistry algorithms,, J. Comput. Chem. 29 (2008) 839–845, https://doi.org/10.1002/jcc.20823.

[57] S. Yadav, N. Goel, V. Kumar, S. Singhal, Graphene oxide as proficient adsorbent for the removal of harmful pesticides: comprehensive experimental cum DFT investigations, Anal. Chem. Lett. 9 (2019) 291–310, https://doi.org/10.1080/22297928.2019.1629999.

[58] H. Wang, B. Hu, Z. Gao, F. Zhang, J. Wang, Emerging role of graphene oxide as sorbent for pesticides adsorption: experimental observations analyzed by molecular modeling, J. Mater. Sci. Technol. 63 (2021) 192–202, https://doi.org/10.1016/j.jmst.2020.02.033.

[59] H. Sajid, S. Khan, K. Ayub, T. Mahmood, Effective adsorption of A-series chemical warfare agents on graphdiyne nanoflake: a DFT study, J. Mol. Model. 27 (2021) 117, https://doi.org/10.1007/s00894-021-04730-3.

[60] H. Ullah, A.-H.A. Shah, S. Bilal, K. Ayub, Doping and dedoping processes of polypyrrole: DFT study with hybrid functionals, J. Phys. Chem. C 118 (2014) 17819–17830, https://doi.org/10.1021/jp505626d.

[61] S. Khan, H. Sajid, K. Ayub, T. Mahmood, Sensing of toxic Lewisite (L 1, L 2, and L 3) molecules by graphdiyne nanoflake using density functional theory calculations and quantum theory of atoms in molecule analysis, J. Phys. Org. Chem. 34;e4181 (2021) 1–12, https://doi.org/10.1002/poc.4181.

[62] S. Khan, H. Sajid, K. Ayub, T. Mahmood, High sensitivity of graphdiyne nanoflake toward detection of phosgene, thiophosgene and phosogenoxime; a first-principles study, J. Mol. Graph. Model. 100 (2020) 107658, https://doi.org/10.1016/j.jmgm.2020.107658.

[63] Z. Fang, Y. Li, J. Li, C. Shu, L. Zhong, S. Lu, C. Mo, M. Yang, D. Yu, in: Capturing Visible Light in Low-Bandgap C4N Derived Responsive Bifunctional Air Electrodes for Solar Energy Conversion/Storage, Angew. Chemie Int, 2021, https://doi.org/10.1002/anie.202104790 anie.202104790.

[64] H. Sajid, K. Ayub, M. Arshad, T. Mahmood, Highly selective acridinium based cyanine dyes for the detection of DNA base pairs (adenine, cytosine, guanine and thymine), Comput. Theor. Chem. 1163 (2019) 112509, https://doi.org/10.1016/j.comptc.2019.112509.

[65] H. Sajid, F. Ullah, K. Ayub, T. Mahmood, Cyclic versus straight chain oligofuran as sensor: a detailed DFT study,, J. Mol. Graph. Model. 97 (2020) 107569, https://doi.org/10.1016/j.jmgm.2020.107569.

[66] H. Sajid, F. Ullah, S. Khan, K. Ayub, M. Arshad, T. Mahmood, Remarkable static and dynamic NLO response of alkali and superalkali doped macrocyclic [hexa-] thiophene complexes; a DFT approach, RSC Adv. 11 (2021) 4118–4128, https://doi.org/10.1039/D0RA08099C.

[67] M. Garcia Hernandez, A. Beste, G. Frenking, F. Illas, Charge decomposition analysis of the chemisorption bond, Chem. Phys. Lett. 320 (2000) 222–228, https://doi.org/10.1016/S0009-2614(00)00160-3.